JGR Space Physics

RESEARCH ARTICLE
10.1029/2018JA026135

Long-Term and Solar Cycle Variation of Galactic Cosmic Rays: Evidence for Variable Heliospheric Turbulence

Pauli Väisänen[1], **Ilya Usoskin**[1,2], **and Kalevi Mursula**[1]

[1]ReSoLVE Centre of Excellence, Space Climate Research Unit, University of Oulu, Oulu, Finland, [2]Sodankylä Geophysical Observatory, University of Oulu, Oulu, Finland

Key Points:
- GCR power spectrum slopes are calculated for 63 years
- Slopes of the spectrum are found to vary with the phase of the solar cycle
- Spectrum is found to be Kolmogorov-like during solar minima and random-walk-like during solar maxima

Correspondence to:
P. Väisänen,
Pauli.Vaisanen@oulu.fi

Citation:
Väisänen, P., Usoskin, I., & Mursula, K. (2019). Long-term and solar cycle variation of galactic cosmic rays: Evidence for variable heliospheric turbulence. *Journal of Geophysical Research: Space Physics*, *124*, 804–811. https://doi.org/10.1029/2018JA026135

Received 26 SEP 2018
Accepted 15 JAN 2019
Accepted article online 19 JAN 2019
Published online 1 FEB 2019

©2019. American Geophysical Union. All Rights Reserved.

Abstract The Sun modulates the flux of galactic cosmic rays (GCR) reaching the Earth's orbit. GCR flux has been measured by ground-based neutron monitors (NMs) for several decades, which provides an interesting long-term monitor of solar activity and the heliospheric magnetic field. Here we study the long-term evolution of the power spectrum of GCR over the last six solar cycles, using the power law slope in the frequency range $5.56 \cdot 10^{-6}$ to $2.14 \cdot 10^{-6}$ Hz (between 50 and 130 hr). We use data from 31 neutron monitors during 1953–2016. We show that the power law slopes vary within the solar cycle, with a Kolmogorov-type slope observed at solar minimum and a random-walk-type slope observed at solar maximum. This implies that the different conditions in the different phases of the solar cycle affect the scaling properties of heliospheric turbulence and, thereby, cosmic ray variability.

1. Introduction

Fluxes of galactic cosmic rays (GCR) recorded by neutron monitors (NMs) at Earth are modulated in the heliosphere by solar activity. Heliospheric modulation of GCR involves four physical processes, namely, diffusion, convection in the radially expanding solar wind, adiabatic cooling, and drifts (for a review, see, e.g., Potgieter, 2013). Diffusion is affected by scattering of GCR on magnetic irregularities of the heliospheric magnetic field (HMF) that are produced by turbulent solar wind (SW) flow. The strength and structure of the HMF vary in time, especially in relation to the 11-year solar cycle and the 27-day solar rotational period. The large-scale properties of SW turbulence are not known from direct measurements but are typically assumed to be scaled by the HMF (Horbury et al., 2005).

Power spectral density (PSD) of a turbulent system typically exhibits a quantifiable power law behavior, indicating turbulence scaling. The log-log power law slope (also called the spectral index) α calculated from PSD estimations is often used to quantify the turbulent behavior of the measured flow parameters, specifically the energy propagation between different scales. For example, the Kolmogorov-like behavior with $\alpha = -5/3$ (Frisch, 1995; Kolmogorov, 1941a, 1941b, 1941c, 1941d) is commonly observed in turbulent flows and is attributed to the kinetic effects of the flow. The Iroshnikov-Kraichnan (Iroshnikov, 1964; Kraichnan, 1965) slope of $\alpha = -3/2$ results from the magnetic effects on turbulence. The slope with $\alpha = -2$ is usually associated with Brownian noise and has also been observed in the HMF when the flow and magnetic field directions are parallel (Goldreich & Sridhar, 1995; Horbury et al., 2008).

Previous studies (Goldstein et al., 1995; Marsch, 1991) have indicated that the power law behavior of the HMF in the frequency range between $4 \cdot 10^{-4}$ and $2 \cdot 10^{-1}$ Hz is mostly Kolmogorov-like, while the behavior of the solar wind flow speed is Iroshnikov-Kraichnan-like (Podesta et al., 2007). Other studies on the HMF PSD (e.g., Borovsky, 2012) have found a solar cycle variation of the spectral slope of HMF measurements.

Except for a few heliospheric missions (e.g., Ulysses, Helios, and Voyager; see; Goldstein et al., 2015; Horbury & Balogh, 2001) most of direct in situ measurements of turbulence are limited spatially to the locations close to the Earth and temporally only to the space era. On the other hand, GCR can be used as a heliospheric probe, whose variability holds a signature of HMF turbulence in a large heliospheric volume, and which has been measured over a longer timescale. Since the GCR flux outside the heliosphere can be assumed constant on the timescale shorter than a million of years, a typical diffusion time of GCR in the galaxy, the variability of GCR flux observed at Earth on centennial and shorter timescales, is driven solely by changes in the heliospheric parameters, reflecting their behavior through the solar cycle. The variability

Table 1
Neutron Monitors Used in the Study: Name, Type, Geographical Coordinates and Altitude, Effective Geomagnetic Cutoff Rigidity, and the Interval of Data Coverage

Monitor	Type	Latitude	Longitude	Altitude (m)	Rigidity (GV)	Data coverage
Alma-Ata	18NM64	43.14°N	76.60°E	3,340	6.69	1973–2016
Alma-Ata 806	6NM64	43.25°N	76.92°E	806	6.61	1973–1999
Apatity	18NM64	67.57°N	33.40°E	181	0.65	1961–2016
Calgary	12NM64	51.08°N	−114.13°W	1,128	1.08	1964–2009
Chicago	12IGY	41.83°N	−87.67°W	200	1.72	1957–1976
Churchill	18NM64	58.75°N	−94.08°W	39	0.21	1957–1976
Climax	12IGY	39.37°N	−106.18°W	3,400	2.99	1953–2006
DeepRiver	18NM64	46.10°N	−77.50°W	145	1.14	1957–1995
Dourbes	18NM64	50.10°N	4.60°E	225	3.34	1969–2015
Goose Bay	18NM64	53.27°N	−60.40°W	46	0.64	1964–2000
Haleakala	18NM64	20.72°N	−156.28°W	3,030	12.91	1991–2006
Huancayo	12IGY	−12.03°S	−75.33°W	3,400	12.92	1953–1992
Inuvik	18NM64	68.35°N	−133.72°W	21	0.17	1964–2016
Irkutsk	12NM64	52.37°N	100.55°E	2,000	3.64	1981–2016
Jungfraujoch	12IGY	46.55°N	7.98°E	3,475	4.49	1966–2016
Kiel	18NM64	54.30°N	−10.10°W	54	2.36	1957–2009
LARC	6NM64	−62.20°S	−58.96°W	40	3.0	1991–2008
Leeds	18NM64	53.80°N	−1.55°W	72	2.20	1957–1983
McMurdo	18NM64	−77.90°S	166.60°E	48	0	1960–2016
Moscow	24NM64	55.47°N	37.32°E	200	2.43	1958–2016
MtWashington	12IGY	44.27°N	−71.30°W	1,909	1.46	1955–1991
Newark	9NM64	39.70°N	−75.70°W	50	2.09	1978–2016
Novosibirsk	24NM64	54.48°N	83.00°E	163	2.91	1971–2016
Oulu	9NM64	65.06°N	25.47°E	15	0.8	1964–2016
Potchefstroom	15IGY	−26.68°S	27.10°E	1,351	7.0	1971–2015
SANAE	6NM64	−71.67°S	−2.85°W	856	0.86	1964–2015
SouthPole	3NM64	−90.00°S	0°	2,820	0.09	1964–2016
Swarthmore	9NM64	39.90°N	−75.35°W	80	1.92	1964–1978
Thule	18NM64	76.60°N	−68.80°W	260	0.0	1957–2016
Tixie	18NM64	71.36°N	128.54°E	0	0.48	1966–2016
Yakutsk	18NM64	62.01°N	129.43°E	105	1.65	1960–2016

of cosmic rays has been systematically recorded by the worldwide network of standard ground-based NMs since 1951 (e.g., Usoskin et al., 2005; Vainio et al., 2009), providing a fairly uniform long-term database.

The PSD of cosmic ray variability was studied, for example, by Kudela and Sabbah (2016) with a special emphasis on quasi-periodicities. However, a comprehensive analysis of the long-term variation of spectral slopes of NM data is still lacking. Here we focus on the long-term and solar cycle variability of the spectral slope of GCR power spectrum, which serves as an index of magnetic irregularities. In this work we present the results of a systematic study of the spectral slope of GCR variability over the last almost six solar cycle (1953–2016), using data from the worldwide NM network. The paper is organized as follows. In section 2 we introduce the data sets and the spectral analysis methods used in the study. Section 3 presents the power spectrum of cosmic rays for the whole period of study and describes the results of long-term evolution of the power law slopes. We study the power law slopes in different solar cycle phases in section 4. We discuss the results and give our conclusions in section 5.

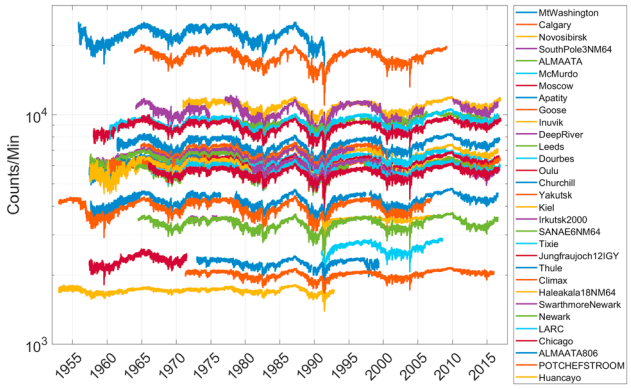

Figure 1. Overview of the different neutron monitor time series used, after removing outliers, ground-level enhancements, and discontinuities. Legends are sorted by mean count rate per minute, from high to low.

2. Data and Methods

2.1. Data

We use count rates from 31 NMs distributed over the globe, covering the years from 1953 to 2016, that is, nearly six full solar cycles. The list of used monitors and their properties is shown in Table 1.

Data were collected from the data server maintained by the Institute of Terrestrial Magnetism, Ionosphere and Radio Wave Propagation (IZMIRAN) at http://cr0.izmiran.ru/common/links.htm, and from the European Neutron Monitor Database at http://nnmdb.eu. All data sets were downloaded at 1-hr resolution, which is sufficient for the frequency range to be studied.

All data were visually inspected for consistency, and the observed inhomogeneities were excluded. Outliers in the data were removed by applying a median filter cutting off data points more than three median absolute deviations (= median($|X_i - \text{median}(X)|$) apart from the running median over the 1,000 nearest data points. Times of ground-level enhancements (GLEs), as given in the international GLE database at http://gle.oulu.fi, were removed from our data. However, Forbush decreases were not removed for this study.

An overview of the data of the 31 NM data sets is shown in Figure 1. Different NMs have different count rates depending on their location (geomagnetic cutoff rigidity), altitude, and type of the NM. The first few years from 1953 to 1957 were covered by only two stations, Climax and Huancayo, with a bunch of new stations launched in the International Geophysical Year in 1957. A new design of a NM was introduced in 1964 as the neutron supermonitor NM64. Most NMs after 1964 are of the NM64 type, which is more effective than the previously used IGY-type design. The number of available monitors during different times are shown in Figure 2.

2.2. PSD Method and Slope Calculation

There are many PSD estimation methods which all have their advantages and disadvantages. Here we used Thomson's multitaper method (Thomson, 1982), which produces PSD estimates with less variance than other methods, at the cost of extended computation time. In the multitaper method, the studied signal data is windowed/tapered multiple times separately using orthogonal tapers obtained from Slepian sequences. Each taper produces one PSD estimate, which are then averaged to obtain the final multitaper PSD estimate, using the default adaptive frequency-dependent weighting described in Percival and Walden (1993; Matlab function pmtm, Mathworks, 2005). Since the tapers determined by the Slepian sequences introduced by Slepian (1978) (also called discrete prolate spheroidal sequences, DPSS) are orthogonal, all the PSD estimates are statistically independent. We selected to use 13 tapers in our study, based on tests using different numbers of tapers. One specific feature of the multitaper method is the widening of signal peaks so that the peak power can leak to nearby frequencies. This is not an issue here, since we study the power law behavior in the frequency range which is quite far away from any notable peaks. A review of the multitaper method with comparison to other common PSD methods can be found in Babadi and Brown (2014). The most practical advantage in our case is the reduced level of noise in the PSD, which allows shorter intervals of data than, for example, the Welch method.

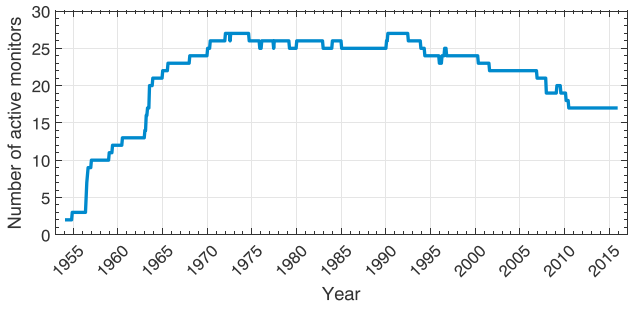

Figure 2. Number of available neutron monitors during each 27 Bartels rotations.

In this study, the power law slopes were calculated assuming that the relation between PSD power P and frequency f is a power law within the selected frequency range

$$P = 10^b \cdot f^{\alpha}, \tag{1}$$

where α is the power law slope and b is another fit parameter. Here α is a negative quantity, meaning that higher values of α correspond to a flatter spectral slope and lower values to a steeper one. The fit was performed

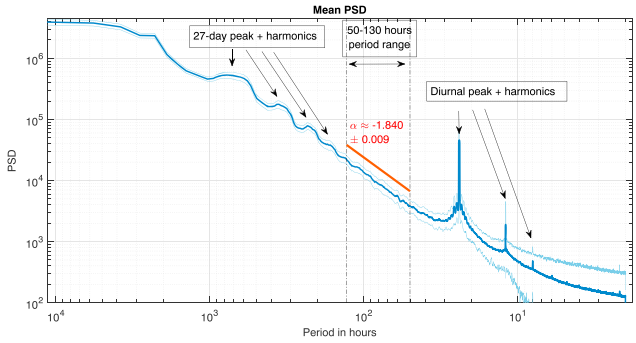

Figure 3. Mean power spectral density (PSD) of all the calculated PSDs (blue). Standard deviation limits are shown in light blue. The studied period range is indicated by the vertical dash-dotted line. The slope fit of the mean PSD is shown red. The diurnal and 27-day peaks are indicated by arrows.

applying a modified (see later) least squares method in log-log coordinate system. In our case the use of the least squares method is validated by the fact that the PSD values are observed to be nearly lognormally distributed.

For the fit, we have selected the frequency range of $5.56 \cdot 10^{-6}$ to $2.14 \cdot 10^{-6}$ Hz, corresponding to the period range from 50 to 130 hr as shown in Figure 3. The amount of frequency data points for calculation is 140. The above mentioned part of the spectrum lies between two major peaks, the diurnal peak and the 27-day solar rotation peak, and has the clearest power law behavior that can be found in the GCR power spectrum. The mean of all calculated PSDs in Figure 3 outlines this frequency range.

The PSDs and their spectral slopes were computed by applying the following procedure:

1. For each NM, data for a time interval of 27 Bartels rotations long (≈2 years) was selected. For shorter time intervals the variance of slopes was fairly large.
2. If a station's data coverage for a given 27-rotation interval was less than 65%, the station was omitted for this interval. The average fraction of data sets with the >65% coverage was 91% before the year 1965 and 95% after 1965. The data were linearly interpolated between data gaps. The total amount of missing data points was around 6.5%. Of all the data gaps, 42% were 1-hr long (=1 data point), 45% were between 2- and 10-hr long, and 13% were longer than 10 hr in length.
3. The data were then linearly detrended and standardized (first remove the mean and then divide by standard deviation).
4. The PSD was calculated using the multitaper method with 13 Slepian sequence tapers. This number of tapers gives an accurate spectrum with a reasonable computation time without too much leakage of power to neighboring frequencies.
5. The spectral slope was calculated using the weighted linear regression in the log-log coordinates. Since the fit is done logarithmically, the resulting least squares fit gives a disproportionally high weight to higher frequencies because of the higher amount of data points (roughly 2.6 times more data point density at $2.14 \cdot 10^{-6}$ Hz than at $5.56 \cdot 10^{-6}$ Hz). To compensate for this, we used a weighted linear regression, where the full weight of one was given to the data point at the lowest frequency, and smaller weight (inversely proportional to the data point density) given to other data points (i.e., the last data point has a weight of $1/2.6 = 0.385$). This method ensures that the fit is not overdominated by higher frequencies.
6. The time window was moved forward by one Bartels rotation (27 days) and the above steps were repeated starting from the original data.

3. Long-Term Evolution of the Spectral Slope

3.1. Power Spectrum of Cosmic Rays

The mean PSD of GCR variability for the entire interval of 1953–2016, computed as the logarithmic mean of all available PSDs for each 27-rotation (spanning about 2 years of data), is shown in Figure 3. The PSDs

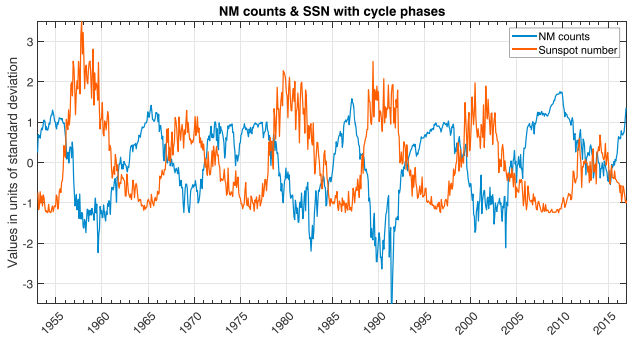

Figure 4. Standardized (first remove the mean and then divide by standard deviation) neutron monitor (NM) count rate (blue) and sunspot number (SSN, red).

were first averaged monitor-wise to ensure that possible monitor-specific effects on PSDs of long-lived monitors are not overemphasized. Two main periodicities in the PSD in the depicted period range are the 27-day solar rotation peak and the diurnal peak and their harmonics. Between these peaks lies the studied period range of 50 to 130 hr, depicting a fairly clear power law behavior. For this period range we obtained the mean slope value of -1.840 ± 0.009 from the mean PSD. Results of -1.83 ± 0.01 (Kudela & Sabbah, 2016) and -1.91 (Attolini et al., 1975) from earlier work are fairly close to this result, albeit the differences in the studied frequency ranges and times.

3.2. Long-Term Evolution of Slope

Figure 4 shows the average of standardized NM count rates and sunspot numbers. One can see the well-known dominant 11-year solar cycle in GCR, roughly in antiphase with sunspot numbers, upon which short-term fluctuations are superposed.

Figure 5 shows power law slopes computed in each 27-rotation interval as described in Section 2. The corresponding solar cycle phases are indicated by the colored bars in the bottom of the panel. Mean values for each 27-day interval are shown in purple. The light blue areas around the mean indicate the standard deviation.

The mean slopes vary significantly between the values of -1.0 and -2.5. The highest slope values (the flattest spectra) above -1.4 are found around years 1964, 1975, and 1986, which are close to the minima of cycles 19, 20, and 21, respectively. High slope values also appear close to the minima of cycles 22 and 23, but their values are close to -1.6. The lowest mean slopes (the steepest spectra) of below -2.2 are found around years 1970, 1978, 1992, and 2015. These years correspond to maximum or early declining phase of the solar cycle, with the exception of 1978, which is an ascending phase year.

4. Solar Cycle Phase Dependence of Slope

We have studied the slope values during different solar cycle phases (see Table 2). We ascribed the slope values to a specific phase of a cycle according to the center of the 27-rotation time interval for which the slope was calculated. The division of the years to cycle phases was partly based on the work of Hathaway (2015) and partly on additional information about the occurrence of high-speed solar wind streams (Mursula et al., 2015) and about the level of cosmic ray intensity. Years 1973-1974 were not ascribed to any solar cycle phase because of the unusual CR modulation during these years (the so called "minicycle," see, e.g., Webber & Lockwood, 1988). Year 2003 was also hard to differentiate between solar cycle maximum and declining phase (for example, the decline in sunspot numbers is not observed in NM counts), so it was left out of the analysis.

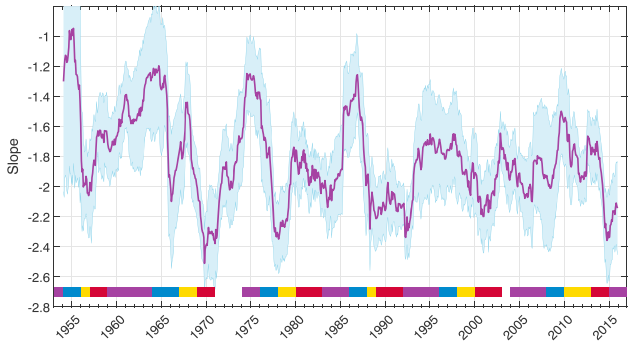

Figure 5. Mean power spectral density slope value (purple) over 2-year overlapped slopes at time scales between 130 and 50 hr for each 27-rotation interval. 1σ standard deviation limits are denoted by light blue. Color bars in the bottom show the declining (purple), minimum (blue), ascending (yellow), and maximum (red) solar cycle phases (see Table 2).

For each cycle phase, we calculated the mean value of all the slopes associated to this phase and the kernel density estimations (KDEs) with a width of 0.06 of the slope distribution. KDE produces a smooth distribution function, in contrast to usual histograms whose discrete values depend on binning. Instead of assigning values to a selected bin, KDE creates a continuous Gaussian (or another type) distribution around each point, which are finally summed together.

Figure 6a depicts the mean and median values of the slopes for each cycle phase, and Figure 6b the corresponding KDEs. One can see that KDEs are different for the different phases. The slope mean value is lowest (-2.03)

Table 2
Division of Years Into Solar Cycle Phases

Cycle	Ascending	Maximum	Declining	Minimum
18	—	—	1953	1954, 1955
19	1956	1957, 1958	1959, 1960, 1961, 1962, 1963	1964, 1965, 1966
20	1967, 1968	1969, 1970	1974, 1975	1976, 1977
21	1978, 1979	1980, 1981, 1982	1983, 1984, 1985	1986, 1987
22	1988	1989, 1990, 1991	1992, 1993, 1994, 1995	1996, 1997
23	1998, 1999	2000, 2001, 2002	2004, 2005, 2006, 2007	2008, 2009
24	2010, 2011, 2012	2013, 2014	2015, 2016	–

during solar maximum, and highest (−1.69) for solar minimum. Ascending and declining phases have the mean slope values of −1.91 and −1.78, respectively. Note that this range of slope values is interesting, ranging from the Brownian noise (slope −2) around solar maxima to the Kolmogorov-type spectrum around solar minima. We also note that the mean and median values are close to each other, especially during solar maxima, implying a fairly symmetric distribution.

The slope KDE distributions (Figure 6b) are quite wide, but distinguishably different for different cycle phases. For example, the slope hardly gets above −1.4 for the maximum phase, but for the declining and minimum phases it is distributed more evenly and extends to higher values up to −0.8 and above. Most KDE distributions peak at around −2, but the distributions vary differently around their maxima. For the solar cycle maximum the peak is quite narrow and higher than in other phases, but slightly asymmetric, with low values between −2.4 and −2.2 being overrepresented compared to those between −1.8 and −1.6.

The KDE of the ascending phase is rather broad and fairly symmetric around the peak value. It has almost a Gaussian shape, leading to the closely similar mean and median values. On the contrary, the KDE of the declining phase has a very asymmetric shape. The distribution peaks at around −2.0, but declines rapidly for lower slopes. The mean and median values differ from each other and are much higher than the maximum of the distribution because distribution extends high above −0.8. The distribution for solar minima peaks at around −1.7, but is more symmetric than the KDE of the declining phase.

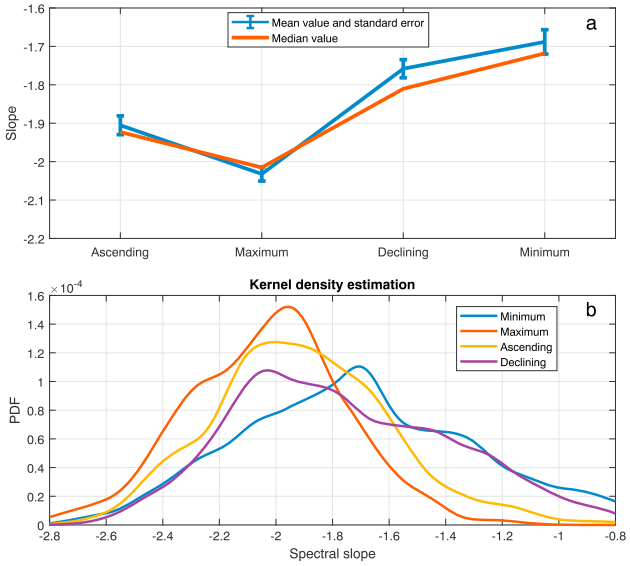

Figure 6. (a) Mean values and standard errors (blue) and median (red) of slope values at different solar cycle phases. (b) Kernel density estimation of slope values during different solar cycle phases.

5. Discussion and Conclusions

We have calculated the power spectral densities and their power law slopes for cosmic rays, as recorded by the worldwide network of neutron monitors of 31 NM stations covering the period of 1953–2016. The slopes were obtained in the frequency range corresponding to timescales from 50 to 130 hr with a total number of calculated PSDs of 16,660. The mean power spectral density has a slope of -1.840 ± 0.009, which agrees with some previous results (e.g., Attolini et al., 1975; Kudela & Sabbah, 2016). Kudela and Sabbah (2016) obtained a power law slope of -1.83 ± 0.01 for the period range between 10,000 and 2 days using data from Climax NM from years 1953 to 2006, which was extended by Lomnicky Stit NM data to 2013. Since this study did not account for the fitting bias toward higher frequencies, the period range studied by Kudela and Sabbah is effectively quite similar to ours. Moreover, the two studies found a similar overall slope value within 2 standard deviations.

Attolini et al. (1975) studied the PSD slope values for the period 1966–1968 using only a few neutron monitors. Slope values for individual NM's varied from −1.812 to −2.045 with the mean of −1.91 for the period range from 911 to 29 hr. These values fall within 1 sigma of our slope of −1.766 for 1967 (see Figure 5). The lower mean value obtained by them can be due to the different period range, containing the solar rotational peak at around 27 days, which may distort the result.

These earlier studies were focused on finding a single power law slope value for a long period. Our results point out that the slope value changes noticeably with the solar cycle. Thus, a single slope value calculated over a long time period may not portray real behavior of the PSD, but rather it will be a mix of multiple different types of spectra with different slopes.

The time evolution of the slopes depicts an interesting pattern over the solar cycle. The spectra are steeper around solar cycle maxima and flatter around minima. The mean slope values for the ascending, maximum, declining, and minimum solar cycle phases were found to be −1.91, −2.03, −1.78, and −1.69, respectively. Accordingly, the slope values vary between values typical to purely random processes (−2) during the maximum phase and values typical for Kolmogorov-type turbulence (−1.67) during the minimum phase. The ascending phase reminds more closely to the maximum phase situation, while the declining phase is more like the minimum phase.

These results indicate that the heliospheric modulation has a noticeably variable effect on cosmic rays depending on the heliospheric conditions. We suggest that during the solar cycle minimum times, kinetic self-organized turbulence dominates the spectrum of cosmic ray variation. During more active times, especially around solar cycle maximum, random processes and events in the heliosphere, caused by solar activity, particularly eruptive events (CME, CMIR, and GMIR), play a key role.

We also found a long-term change of slope values from solar cycles 20–21 to cycles 22–23. During cycles 20–21, values of the slopes ranged from below −2.4 to above −1.3, whereas for cycles 22–23 the values were much closer to the overall mean value of −1.86, varying between −2.3 and −1.5. This may, at least partly, explain the changed scaling of cosmic ray modulation during solar cycles 23 and 24 (e.g., Usoskin et al., 2017), so that the NM count rate was, in 2009–2010, at a record-high level for polar NMs but not for middle- and low-latitude NMs.

Finally, we note some possible caveats that may affect the presented results. We have calculated the spectral slopes for data obtained by several NMs (only removing the GLE times). Although the effect of the harmonics of the 27-day solar rotation is assumed to be negligible from the fourth harmonic onward, they may cause some change during specific types of solar activity, for example, during strong 27-day periodic "trains." Also, the present results may be partly affected by Forbush decreases, especially during the maximum phase but not for other cycle phases. One should also note that the operation, instrumentation, and assortment of NMs change with time, which may have effects on the long-term data sets and the results. Additionally, we note that there may be a small rigidity dependence of the slopes. Initial tests show that this is a very small effect, which has no effect on the current results. We will study in the future if this rigidity dependence is systematic or not.

In conclusion, we have found that an imprint of solar activity is clearly observed in the variation of the PSD slopes calculated from NM data from years 1953 to 2016. This outlines the need to understand and to account for the long-term solar variation and its impact on of the heliosphere and GCR propagation. The

connection to GCR modulation and energy propagation and dissipation in the heliosphere was not studied in this investigation, but will be left for a future study.

Acknowledgments
We acknowledge the financial support by the Academy of Finland to the ReSoLVE Centre of Excellence (project 307411). Pauli Väisänen acknowledges the personal research grant from the Finnish Cultural Foundation. We thank NMDB (http://nnmdb.eu) and IZMIRAN (http://cr0.izmiran.ru/common/links.htm) for their databases of NM data and all individual neutron monitor teams for access to their data. Oulu NM data are available at http://cosmicrays.oulu.fi.

References

Attolini, M., Cecchini, S., Guidi, I., & Galli, M. (1975). The shape of the power spectrum of cosmic ray at ground level up to 7×10^3 Hz. *Planetary and Space Science*, *23*(12), 1603–1609. https://doi.org/10.1016/0032-0633(75)90088-4

Babadi, B., & Brown, E. N. (2014). A review of multitaper spectral analysis. *IEEE Transactions on Biomedical Engineering*, *61*(5), 1555–1564. https://doi.org/10.1109/TBME.2014.2311996

Borovsky, J. E. (2012). The velocity and magnetic field fluctuations of the solar wind at 1 AU: Statistical analysis of Fourier spectra and correlations with plasma properties. *Journal of Geophysical Research*, *117*, A05104. https://doi.org/10.1029/2011JA017499

Frisch, U. (1995). *Turbulence. The Legacy of A. N. Kolmogorov*. Cambridge, UK: Cambridge University Press. https://doi.org/10.1017/CBO9781139170666

Goldreich, P., & Sridhar, S. (1995). Toward a theory of interstellar turbulence. 2: Strong Alfvenic turbulence. *Astrophysical Journal*, *438*, 763–775. https://doi.org/10.1086/175121

Goldstein, M. L., Roberts, D. A., & Matthaeus, W. H. (1995). Magnetohydrodynamic turbulence in the solar wind. *Annual Review of Astronomy and Astrophysics*, *33*, 283–326. https://doi.org/10.1146/annurev.aa.33.090195.001435

Goldstein, M. L., Wicks, R. T., Perri, S., & Sahraoui, F. (2015). Kinetic scale turbulence and dissipation in the solar wind: key observational results and future outlook. *Philosophical Transactions of the Royal Society of London A: Mathematical, Physical and Engineering Sciences*, *373*, 2041. https://doi.org/10.1098/rsta.2014.0147

Hathaway, D. H. (2015). The solar cycle. *Living Reviews in Solar Physics*, *12*, 4. https://doi.org/10.1007/lrsp-2015-4

Horbury, T. S., & Balogh, A. (2001). Evolution of magnetic field fluctuations in high-speed solar wind streams: Ulysses and Helios observations. *Journal of Geophysical Research*, *106*, 15,929–15,940. https://doi.org/10.1029/2000JA000108

Horbury, T. S., Forman, M. A., & Oughton, S. (2005). Spacecraft observations of solar wind turbulence: an overview. *Plasma Physics and Controlled Fusion*, *47*, B703–B717. https://doi.org/10.1088/0741-3335/47/12B/S52

Horbury, T. S., Forman, M., & Oughton, S. (2008). Anisotropic scaling of magnetohydrodynamic turbulence. *Physical Review Letters*, *101*(17), 175005. https://doi.org/10.1103/PhysRevLett.101.175005

Iroshnikov, P. S. (1964). Turbulence of a conducting fluid in a strong magnetic field. *Soviet Astronomy*, *7*, 566.

Kolmogorov, A (1941a). The local structure of turbulence in an incompressible fluid at very high Reynolds numbers. *Proceedings of the USSR Academy of Sciences*, *30*, 299–303.

Kolmogorov, A (1941b). The logarithmically normal distribution of the size of particles under the fragmentation. *Proceedings of the USSR Academy of Sciences*, *31*, 99–101.

Kolmogorov, A (1941c). The decay of isotropic turbulence in an incompressible viscous fluid. *Proceedings of the USSR Academy of Sciences*, *31*, 538–541.

Kolmogorov, A. (1941d). Energy dissipation in locally isotropic turbulence. *Proceedings of the USSR Academy of Sciences*, *32*, 19–21.

Kraichnan, R. H. (1965). Inertial-range spectrum of hydromagnetic turbulence. *Physics of Fluids*, *8*, 1385–1387. https://doi.org/10.1063/1.1761412

Kudela, K., & Sabbah, I. (2016). Quasi-periodic variations of low energy cosmic rays. *Science China Technological Sciences*, *59*(4), 547–557. https://doi.org/10.1007/s11431-015-5924-y

Marsch, E. (1991). MHD turbulence in the solar wind. *Physics and Chemistry in Space*, *21*, 159–241. https://doi.org/10.1007/978-3-642-75364-0_5

Mathworks (2005). Multitaper power spectral density estimate. Retrieved from https://se.mathworks.com/help/signal/ref/pmtm.html

Mursula, K., Lukianova, R., & Holappa, L. (2015). Occurrence of high-speed solar wind streams over the grand modern maximum. *The Astrophysical Journal*, *801*, 30. https://doi.org/10.1088/0004-637X/801/1/30

Percival, D. B., & Walden, A. T. (1993). Spectral analysis for physical applications. https://doi.org/10.1017/CBO9780511622762

Podesta, J. J., Roberts, D. A., & Goldstein, M. L. (2007). Spectral exponents of kinetic and magnetic energy spectra in solar wind turbulence. *Astrophysical Journal*, *664*, 543–548. https://doi.org/10.1086/519211

Potgieter, M. S. (2013). Solar modulation of cosmic rays. *Living Reviews in Solar Physics*, *10*, 3. https://doi.org/10.12942/lrsp-2013-3

Slepian, D. (1978). Prolate spheroidal wave functions, Fourier analysis, and uncertainty. V—The discrete case. *AT T Technical Journal*, *57*, 1371–1430. https://doi.org/10.1002/j.1538-7305.1978.tb02104.x

Thomson, D. J. (1982). Spectrum estimation and harmonic analysis. *IEEE Proceedings*, *70*(9), 1055–1096. https://doi.org/10.1109/PROC.1982.12433

Usoskin, I. G., Alanko-Huotari, K., Kovaltsov, G. A., & Mursula, K. (2005). Heliospheric modulation of cosmic rays: Monthly reconstruction for 1951–2004. *Journal of Geophysical Research*, *110*, A12108. https://doi.org/10.1029/2005JA011250

Usoskin, I. G., Gil, A., Kovaltsov, G. A., Mishev, A. L., & Mikhailov, V. V. (2017). Heliospheric modulation of cosmic rays during the neutron monitor era: Calibration using PAMELA data for 2006–2010. *Journal of Geophysical Research: Space Physics*, *122*, 3875–3887. https://doi.org/10.1002/2016JA023819

Vainio, R., Desorgher, L., Heynderickx, D., Storini, M., Flückiger, E., Horne, R. B., et al. (2009). Dynamics of the Earth's particle radiation environment. *Space Science Reviews*, *147*, 187–231. https://doi.org/10.1007/s11214-009-9496-7

Webber, W. R., & Lockwood, J. A. (1988). Characteristics of the 22-year modulation of cosmic rays as seen by neutron monitors. *Journal of Geophysical Research*, *93*, 8735–8740. https://doi.org/10.1029/JA093iA08p08735